

**Raman studies of  $A_2MWO_6$  tungstate double perovskites**

Journal:	<i>Dalton Transactions</i>
Manuscript ID:	DT-ART-12-2014-003789.R1
Article Type:	Paper
Date Submitted by the Author:	22-Jan-2015
Complete List of Authors:	Andrews, Rebecca; Ohio State University, Department of Chemistry and Biochemistry Heyns, Anton; Ohio State University, Department of Chemistry and Biochemistry Woodward, Patrick; Ohio State University, Department of Chemistry and Biochemistry

## ARTICLE

## Raman studies of $A_2MWO_6$ tungstate double perovskites

Cite this: DOI: 10.1039/x0xx00000x

R. L. Andrews,<sup>a</sup> A. M. Heyns<sup>a</sup> and P. M. Woodward<sup>a</sup>Received 00th January 2012,  
Accepted 00th January 2012

DOI: 10.1039/x0xx00000x

www.rsc.org/

The Raman spectra of seven  $A_2MWO_6$  tungstate double perovskites are analysed.  $Ba_2MgWO_6$  is a cubic double perovskite with  $Fm\bar{3}m$  symmetry and its Raman spectrum contain three modes that can be assigned in a straightforward manner. A fourth mode, the asymmetric stretch of the  $[WO_6]^{6-}$  octahedron, is too weak to be observed. The symmetry of  $Ba_2CaWO_6$  is lowered to tetragonal  $I4/m$  due to octahedral tilting, but the distortion is sufficiently subtle that the extra bands predicted to appear in the Raman spectrum are not observed. The remaining five compounds have additional octahedral tilts that lower the symmetry to monoclinic  $P2_1/n$ . The further reduction of symmetry leads to the appearance of additional lattice modes involving translations of the A-site cations and librations of the octahedra. Comparing the Raman spectra of fourteen different  $A_2MWO_6$  tungstate double perovskites shows that the frequency of the symmetric stretch ( $\nu_1$ ) of the  $[WO_6]^{6-}$  octahedron is relatively low for cubic perovskites with tolerance factors greater than one due to underbonding of the tungsten and/or M cation. The frequency of this mode increases rapidly as the tolerance factor drops below one, before decreasing gradually as the octahedral tilting gets larger. The frequency of the oxygen bending mode ( $\nu_5$ ) is shown to be dependent on the mass of the A-site cation due to coupling of the internal bending mode with external A-site cation translation modes.

### Introduction

The perovskite family is one of the largest and most important in all of solid state chemistry. Perovskites have a stoichiometry of  $AMO_3$ , and the aristotype structure possesses  $Pm\bar{3}m$  space group symmetry. The M cation resides at the centre of an octahedron, and the A cation occupies the cubooctahedral cavities that exist in the corner connected framework of  $MO_6$  octahedra. Ordering of two unique octahedral cations on a three dimensional checkerboard pattern (i.e. rock salt ordering) leads to the  $A_2MM'O_6$  double perovskite structure, where the unit cell is doubled along all three axes and the space group symmetry becomes  $Fm\bar{3}m$ . Double perovskites are a large group of compounds numbering more than 1000 [1-3]. They are prized for a variety of properties and are used as relaxor ferroelectrics [4], microwave dielectrics [5], ionic conductors [6], and half-metallic conductors [7].

Most perovskites do not adopt the aristotype cubic structure, but are distorted in some manner. The most common type of distortion in perovskites is octahedral tilting [2, 3, 8, 9, 10]. When the tolerance factor is less than one, the size of the A-site cation is too small for its cubooctahedral cavity and cooperative tilts of essentially rigid octahedra are expected. Octahedral tilting modifies the coordination environment of the A-site cation while maintaining the octahedral coordination

environment of the M and M' cations. At the same time it lowers the overall symmetry of the crystal structure.

There are many examples in the literature of incorrect structure determinations that stem from an inability to correctly identify the correct pattern of octahedral tilting. This is particularly true for double perovskites because the diffraction peaks that arise from rock salt ordering of M and M' ions are the same as those that arise from out-of-phase tilting of the octahedra [11, 12]. In some instances neutron diffraction studies are needed to make definitive space group assignments, which can be problematic because access to neutron scattering facilities is limited.

Raman spectroscopy is an alternative technique for monitoring the reduction in symmetry that accompanies octahedral tilting. In theory additional bands should appear as the symmetry is lowered, but in practice it is not always possible to see all of the additional bands in spectra taken on polycrystalline samples. In this paper Raman spectroscopy is used to probe the local structure of seven  $A_2M^{2+}WO_6$  double perovskites. The compounds studied were chosen to meet several criteria. By choosing perovskites whose tolerance factors range from 1.038 ( $Ba_2MgWO_6$ ) to 0.867 ( $Ca_2CaWO_6$ ) the group contains compounds with various patterns of octahedral tilting. Because the oxidation states of the M and M' ions differ by four, the presence of antisite disorder, which can complicate interpretation of Raman spectra, can be avoided. By

systematically analysing the Raman spectra of these compounds the links between changes in crystallographic symmetry and the appearance of new bands in the Raman spectra are revealed. By limiting the study to a set of perovskites where the strongest bonding unit, the  $[\text{WO}_6]^{6-}$  octahedron, remains constant we can study the effect of changes in composition, bonding, and structure on the frequencies and intensities of the internal vibrations of the  $[\text{WO}_6]^{6-}$  octahedron.

## Experimental

All samples were prepared using conventional solid state synthesis methods. High purity (>99%) starting materials of  $\text{BaCO}_3$ ,  $\text{SrCO}_3$ ,  $\text{CdO}$ ,  $\text{MgO}$ ,  $\text{ZnO}$ ,  $\text{CaCO}_3$ , and  $\text{WO}_3$  were used. Stoichiometric amounts of the starting materials were ground in an agate mortar and pestle before heating in ceramic crucibles for 12 – 24 hours. Multiple heating cycles with intermittent grinding were necessary for some materials. The annealing temperature was 950 °C for  $\text{Sr}_2\text{CdWO}_6$ , 1000 °C for  $\text{Sr}_2\text{ZnWO}_6$ , 1200 °C for  $\text{Ca}_2\text{CaWO}_6$ , and 1300 °C for the remaining compounds. X-ray powder diffraction patterns were collected with a Bruker D8 Advance X-ray diffractometer (40 kV, 50 mA, copper source  $\lambda = 1.5406 \text{ \AA}$ ). Rietveld refinements of the X-ray diffraction data were performed using Topas Academic software [13]. All Raman studies were performed using a Renishaw Smith Raman IR microprobe with a 514 nm Argon ion laser.

In some samples a few percent of an  $\text{AWO}_4$  ( $A = \text{Sr}, \text{Ba}$ ) secondary phase was detected by X-ray diffraction. To identify any peaks in the Raman spectra that come from the scheelite phases, phase pure samples of  $\text{BaWO}_4$ ,  $\text{SrWO}_4$  and  $\text{CaWO}_4$  were synthesized following the same conventional solid state synthesis method with an annealing temperature of 1100 °C. The Raman spectra of the scheelite tungstates are given in the supporting information.

## Results

### Crystal structures

Throughout this paper octahedral tilting will be described using the tilt system notation developed by Glazer [14]. The  $a^0a^0a^0$  tilt system is the aristotype cubic structure with  $Fm\bar{3}m$  space group symmetry, while the other three tilt systems encountered in tungstate double perovskites are illustrated in Figure 1.

The tilt systems reported in the literature, both at ambient conditions and as a function of temperature, are summarized in Table 1. There is some controversy regarding assignment of tilt systems in  $\text{Ba}_2\text{CaWO}_6$ . Yamamura *et al.* assigned the 220 K phase transition as being driven by a change from monoclinic  $I2/m$  symmetry ( $a^-a^-c^0$  tilting) to tetragonal  $I4/m$  symmetry ( $a^0a^0c^-$  tilting) [15], while Fu *et al.* claimed the transition was actually from  $I4/m$  symmetry to cubic  $Fm\bar{3}m$  symmetry ( $a^0a^0a^0$  tilting) [16]. Day *et al.* later investigated the room temperature structure using both X-ray and neutron diffraction and

concluded that the symmetry at room temperature was tetragonal  $I4/m$  [17]. Therefore, the assignment originally put forward by Yamamura *et al.* seems most credible and is given in Table 1. However, there is a possibility that the symmetry of this compound might be sample dependent.

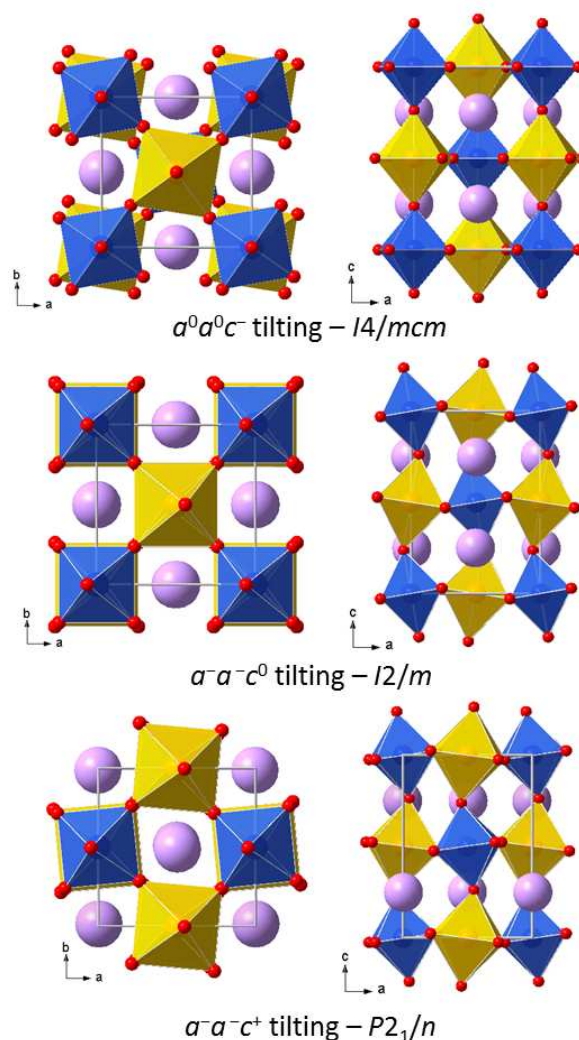


**Figure 1:** The structure of a double perovskite with  $a^0a^0c^-$  (upper),  $a^-a^-c^-$  (middle), and  $a^-a^-c^+$  (lower) tilting.

The X-ray diffraction patterns illustrating the phase purity and peak splitting characteristic associated with various types of octahedral tilting are shown in Figure 2. Rietveld refinements yielded lattice parameters that are in good agreement with those already reported in the literature, as shown in the supporting information (Table S1) [15, 17-20]. The atomic coordinates for six of the seven compounds have previously been determined from neutron powder diffraction data, thus the values obtained in our refinements are not reported here. The lone exception is  $\text{Sr}_2\text{CdWO}_6$ , where the high neutron absorption cross section of cadmium makes neutron diffraction studies impractical. The refined atomic positions for  $\text{Sr}_2\text{CdWO}_6$  can be found in Table 2 and the refined diffraction pattern is shown in Figure 3. The

monoclinic symmetry and atomic coordinates are in good agreement with those reported by Gateshki, *et al.* [18].

**Table 1:** The tolerance factors, tilt system at 300 K, and phase transitions that have been identified in the  $A_2MWO_6$  perovskites under study.

Composition	Tolerance factor ( $t$ )	Octahedral tilting
$Ba_2MgWO_6$ <sup>17</sup>	1.038	$a^0a^0a^0$ (at 300 K)
$Sr_2ZnWO_6$ <sup>17</sup>	0.976	$a^-a^-c^+ \xrightarrow{343\text{ K}} a^0a^0c^-$
$Ba_2CaWO_6$ <sup>15,17</sup>	0.972	$a^-a^-c^0 \xrightarrow{220\text{ K}} a^0a^0c^-$
$Sr_2CdWO_6$ <sup>18,19</sup>	0.930	$a^-a^-c^+ \xrightarrow{1070\text{ K}} a^0a^0c^-$
		$\xrightarrow{1230\text{ K}} a^0a^0a^0$
$Ca_2MgWO_6$ <sup>20</sup>	0.926	$a^-a^-c^+$ (at 300 K)
$Sr_2CaWO_6$ <sup>19</sup>	0.917	$a^-a^-c^+ \xrightarrow{1130\text{ K}} a^0a^0c^-$
		$\xrightarrow{1250\text{ K}} a^0a^0a^0$
$Ca_2CaWO_6$ <sup>17</sup>	0.867	$a^-a^-c^+$ (at 300 K)

During the synthesis of these particular tungsten based perovskites, it was difficult to completely eliminate all traces of a scheelite ( $A^{2+}WO_4$ ) secondary phase, as can be seen by close inspection of Figure 2. Most samples contained less than 1% by mass, but  $Sr_2MgWO_6$  and  $Sr_2CdWO_6$  had approximately 3% and 2% by mass, respectively. The presence of  $AWO_4$  crystallites at such low levels is not likely to impact the crystallography in any meaningful way. However, it is important to identify these phases because as will be seen later, weak bands associated with the scheelite phases are observed in many of the Raman spectra.

**Table 1:** Refined atomic positions for  $Sr_2CdWO_6$  as obtained from Rietveld refinement of powder diffraction data. The goodness of fit was  $\chi^2 = 1.148$ .

Atom	Site	x	y	z	$B_{eq}^*$
Sr	4e	0.0074(4)	0.5371(9)	0.2520(5)	0.577(7)
Cd	2c	0.5	0.5	0	0.402(9)
W	2d	0	0	0	0.402(9)
O1	4e	0.0700(9)	0.0142(5)	-0.2312(5)	1.003(0)
O2	4e	0.2604(9)	-0.1883(2)	0.0300(2)	1.003(0)
O3	4e	0.1812(5)	0.2665(4)	0.0444(0)	1.003(0)

\*The  $B_{eq}$  values for Cd and W were constrained to be the same, as were the  $B_{eq}$  values of O1, O2, and O3.

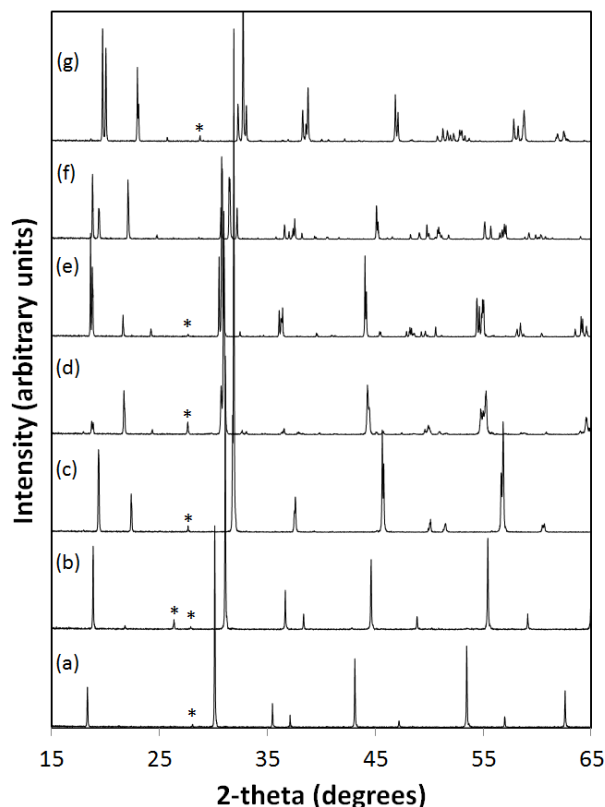


**Figure 2:** X-ray diffraction patterns of (a)  $Ba_2CaWO_6$ , (b)  $Ba_2MgWO_6$ , (c)  $Sr_2ZnWO_6$ , (d)  $Sr_2CdWO_6$ , (e)  $Sr_2CaWO_6$ , (f)  $Ca_2CaWO_6$  and (g)  $Ca_2MgWO_6$ . The peak splitting that results from octahedral tilting can clearly be seen in (c) through (g). The strongest peaks due to the secondary  $AWO_4$  scheelite phases are marked with an asterisk.

To better understand how changes in structure impact the Raman spectra that will be presented in the next section the M–O–W bond angles, mean octahedral bond lengths, and distortion indices  $\Delta_d$  are reported in Table 3. The distortion index ( $\Delta_d$ ) measures the degree to which the M–O and W–O bond distances are distorted from those found in a perfect octahedron. The distortion index is calculated as follows:

$$\Delta_d = \frac{1}{6} \sum_{n=1-6} \left[ \frac{d_n - \langle d \rangle}{\langle d \rangle} \right]^2$$

where  $d_n$  is an individual M–O bond length and  $\langle d \rangle$  is the average M–O bond length. Octahedra with significant distortions of the bond lengths (e.g. those containing Jahn Teller ions like  $Mn^{3+}$ ) have  $\Delta_d$  values greater than  $10^{-3}$  [17, 22]. As can be seen in Table 3 the values of  $\Delta_d$  are generally quite small here, confirming the picture that these structures can be described by tilts of nearly rigid octahedra. The largest distortion occurs in  $Sr_2CdWO_6$ , but given the larger uncertainties associated with determining the structure using laboratory X-ray diffraction it's quite possible that the values of  $\Delta_d$  are overestimated in  $Sr_2CdWO_6$ . The next largest distortion occurs for the Ca-centered octahedra in  $Ca_2CaWO_6$  ( $\Delta_d =$

$1.16 \times 10^{-4}$ ). This distortion is also present in the internal bond angles of the calcium octahedron:  $O1-Ca-O3 = 94.83^\circ$  and  $O2-Ca-O3 = 95.08^\circ$ . According to Day *et. al.*, this can be attributed to the large octahedral tilting distortion and relatively ionic Ca–O bonds, conditions where the assumption of cooperative tilting of truly rigid octahedra starts to break down [17].

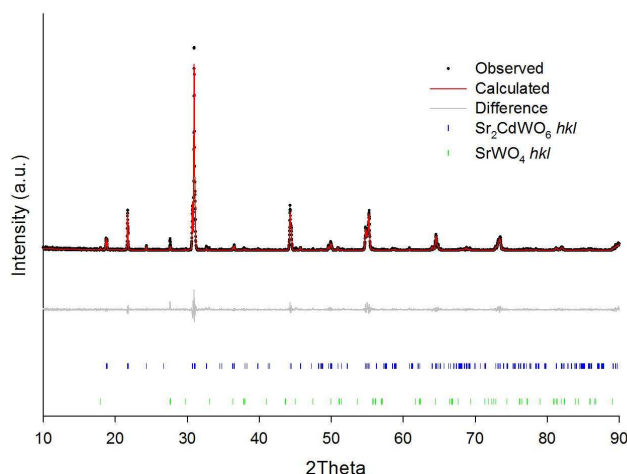


**Figure 3:** Rietveld refinement of  $Sr_2CdWO_6$ . The upper (blue) and lower (green) set of hash marks, denote the position of the  $Sr_2CdWO_6$  and  $SrWO_4$  reflection positions, respectively.

The average W–O distance is fairly constant for all seven compounds, as would be expected, with  $Sr_2CdWO_6$  once again showing up as somewhat of an outlier. The M–O–W bond angles, which are linear in the cubic perovskite structure, become increasingly bent as the tolerance factor decreases and the octahedral tilting becomes more pronounced. The fact that the Ca–O2–W bond in  $Ba_2CaWO_6$  is nearly linear indicates that this compound is on the verge of a phase transition to the undistorted  $Fm\bar{3}m$  structure.

**Table 3:** Select bond distances, bond angles and octahedral distortion indices for the  $A_2MWO_6$  perovskites under study. All parameters determined from previous neutron powder diffraction studies, with the exception of  $Sr_2CdWO_6$ .

Composition	Mean M–O distance (Å)	M <sup>2+</sup> distortion index ( $\times 10^5$ )	Mean W–O distance (Å)	W <sup>6+</sup> distortion index ( $\times 10^5$ )	M–O–W bond angles ( $^\circ$ )
$Ba_2MgWO_6$ <sup>17</sup>	2.123	0	1.929	0	180
$Sr_2ZnWO_6$ <sup>17</sup>	2.084	0.16	1.918	0.11	167.6 165.4 164.1
$Ba_2CaWO_6$ <sup>17</sup>	2.281	2.3	1.920	3.5	180 176.0 157.1
$Sr_2CdWO_6$	2.274	22	1.899	15	158.5 152.1 152.3
$Ca_2MgWO_6$ <sup>20</sup>	2.069	1.1	1.922	1.9	151.1 152.1 153.9
$Sr_2CaWO_6$ <sup>21</sup>	2.339	6.6	1.911	2.5	149.1 147.1 147.2
$Ca_2CaWO_6$ <sup>17</sup>	2.304	12	1.926	1.4	140.9 141.4

#### Raman spectra of $Ba_2MWO_6$ (M = Ca, Mg) double perovskites

Group theory analysis for a double perovskite with the aristotype cubic  $Fm\bar{3}m$  structure shows that there are four Raman active bands expected,  $\Gamma = \nu_1(A_{1g}) + \nu_2(E_g) + \nu_5(F_{2g}) + T(F_{2g})$ , where  $\nu_1$ ,  $\nu_2$ , and  $\nu_5$  are the internal vibration modes of an octahedron and  $T$  is a lattice mode. The  $\nu_1$  mode is the symmetric oxygen stretch vibration of the octahedra, during which all cations are at rest and the oxygen atoms are moving along the M–O–W axis [23]. It appears as a strong, relatively broad peak in the region of 750–850  $cm^{-1}$  [23, 24]. Just as there is an oxygen symmetric stretch, there is also an oxygen asymmetric stretching vibration, labelled as the  $\nu_2$  mode. Again, during a  $\nu_2$  vibration, all cations are at rest while the oxygen atoms vibrate along the M–O–W axes [23]. The internal  $\nu_5$  mode is due to an oxygen bending motion of the octahedron. The  $\nu_2$  and  $\nu_5$  modes are expected to occur in the ranges 470–610  $cm^{-1}$  and 350–490  $cm^{-1}$  respectively [23, 24].

Low energy lattice modes can be classified as external modes (i.e. not associated with the internal vibration of an octahedron) [25]. The external  $T$  modes found in the 100–300  $cm^{-1}$  region arise from translations of the A cation, and are referred to as translational lattice modes [23]. The librational modes,  $L$ , which are also considered lattice modes, can be described as rotations of rigid octahedra. When the crystal has  $Fm\bar{3}m$  symmetry, as  $Ba_2MgWO_6$  does, the librational mode of  $F_{1g}$  symmetry is silent and there is a single Raman active translational mode,  $T(F_{2g})$ .

In the Raman spectrum of  $Ba_2MgWO_6$  (see Figure 4), the peaks at 126, 441, and 812  $cm^{-1}$  are assigned to  $T(F_{2g})$ ,  $\nu_5(F_{2g})$ , and  $\nu_1(A_{1g})$  modes, respectively. The  $\nu_2$  asymmetric stretching mode is too weak to be seen, but is calculated to occur at 540–550  $cm^{-1}$  in normal coordinate calculations using a Urey-Bradley



force field. Its intensity is likewise calculated to be approximately 8% of the  $\nu_1(A_{1g})$  mode. As we will see a very weak  $\nu_2$  mode is not unusual for these ordered double perovskites. These values and assignments are in good agreement with those reported by Liegeois-Duyckaerts and Tarte [23].

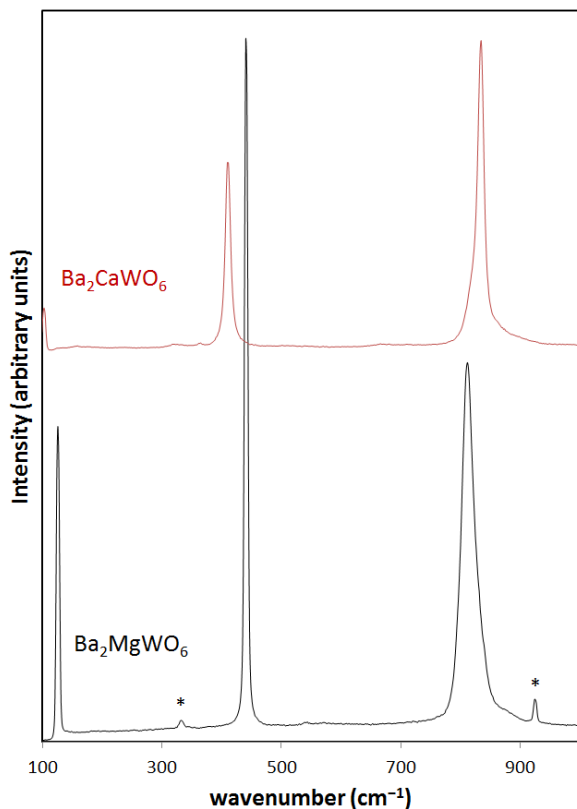


**Figure 4:** Raman spectra of  $\text{Ba}_2\text{MgWO}_6$  and  $\text{Ba}_2\text{CaWO}_6$ . The peaks marked with an asterisk are due to the scheelite phase  $\text{BaWO}_4$ .

When lowering the symmetry to  $I4/m$ , as is the case for  $\text{Ba}_2\text{CaWO}_6$ , additional Raman bands are allowed. The irreducible representation, considering only Raman active vibrations, for a double perovskite with  $I4/m$  symmetry is  $\Gamma = \nu_1(A_g) + \nu_2(A_g + B_g) + \nu_5(B_g + E_g) + T(B_g + E_g) + L(A_g + E_g)$ , which corresponds to nine Raman active modes. However, as shown in Figure 4, only three bands are visible with the lowest energy band falling at the extreme low energy range that can be accessed with our spectrometer. There are various reasons that could be responsible for the absence of extra bands predicted by group theory on lowering the symmetry from  $Fm\bar{3}m$  to  $I4/m$ : (1) bands may be so weak that they are not detected above the background, (2) bands may overlap to such an extent that we are not able to resolve the splitting of the bands, or (3) new bands may fall at energies lower than  $100\text{ cm}^{-1}$ .

The bands appearing at approximately  $834$ ,  $410$ , and  $103\text{ cm}^{-1}$  can be assigned to  $\nu_1$ ,  $\nu_5$ , and  $T$  modes respectively for  $\text{Ba}_2\text{CaWO}_6$ , although there is some uncertainty in the frequency of the band seen at  $103\text{ cm}^{-1}$  because it falls at the very edge of

the accessible range of our spectrometer. As was the case for  $\text{Ba}_2\text{MgWO}_6$  the asymmetric stretch,  $\nu_2$ , is too weak to be observed. Furthermore, the predicted splitting of the  $\nu_5$  mode is too small to be resolved. This is presumably because the degree of distortion from the cubic structure is quite small in  $\text{Ba}_2\text{CaWO}_6$ , (see the bond angles and distances in Table 3). The libration modes  $L$  and the additional  $T$  mode are either too weak to see or fall outside of the spectral range of our spectrometer. Liegeois-Duyckaerts and Tarte observed very similar bands ( $838$ ,  $413$ ,  $105\text{ cm}^{-1}$ ) and from the presence of just three Raman bands concluded that  $\text{Ba}_2\text{CaWO}_6$  was cubic [23]. However, as discussed above careful diffraction studies later showed that the true symmetry was tetragonal  $I4/m$  [15, 17]. So in this case it appears that Raman spectroscopy is no more sensitive, perhaps less so, than X-ray powder diffraction for detecting the subtle lowering in symmetry.

### Raman spectra of monoclinic $\text{A}_2\text{MWO}_6$ double perovskites

The remaining five compounds have additional octahedral tilting distortions (tilt system  $a^-a^-b^+$ ) that lower the symmetry to the monoclinic space group  $P2_1/n$ . Considering only Raman active modes, the irreducible representation for a  $P2_1/n$  perovskite can be written as  $\Gamma = \nu_1(A_g + B_g) + \nu_2(2A_g + 2B_g) + \nu_5(3A_g + 3B_g) + T(3A_g + 3B_g) + L(3A_g + 3B_g)$ . There are now a total of 24 bands predicted to be present in the Raman spectrum, however, in the five compounds studied here only seven to thirteen bands are experimentally observed (see Table 4). In these structures there are two  $\text{A}_2\text{MWO}_6$  formula units per unit cell, and this leads to the presence of  $A_g$  and  $B_g$  components for all of the modes. It would not be unexpected if the  $A_g$  and  $B_g$  components of the internal modes fell at a very similar frequencies, in which case polarized Raman spectra of single crystals may be needed to resolve them. If that is the case spectra collected on polycrystalline samples, as is the case here, should exhibit a single band for the symmetric stretch  $\nu_1$ , a doublet for the asymmetric stretch  $\nu_2$ , and a triplet for the bending mode  $\nu_5$ .

The Raman spectra of the monoclinic double perovskites are shown in Figure 5. An intense oxygen symmetric stretch band,  $\nu_1$ , is seen in each spectrum at values ranging from  $811$  to  $855\text{ cm}^{-1}$ . Unlike  $\text{Ba}_2\text{CaWO}_6$  and  $\text{Ba}_2\text{MgWO}_6$ , the oxygen asymmetric stretching mode,  $\nu_2$ , can be seen in these compounds, but it is so weak that it's not possible to detect splitting of this band without polarized Raman data. The peak at approximately  $918\text{ cm}^{-1}$  in the  $\text{Sr}_2\text{CdWO}_6$  spectrum is assigned to  $\text{SrWO}_4$ . Not only is this where the strongest band in the Raman spectrum of  $\text{SrWO}_4$  is observed (see supporting information), the presence of a peak from the secondary scheelite phase is not unexpected given the presence of  $\text{SrWO}_4$  in the XRD pattern of  $\text{Sr}_2\text{CdWO}_6$ . Very weak  $\text{AWO}_4$  scheelite peaks can also be seen in the spectra of several other compounds.

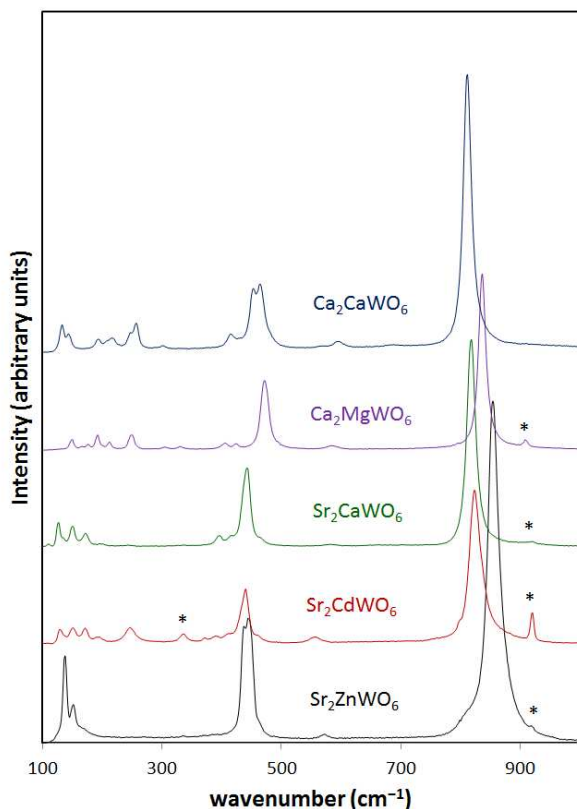


**Figure 5:** Raman spectra of five tungsten-based perovskites with space group  $P2_1/n$ . The peaks marked with an asterisk are due to the scheelite secondary phase, either  $SrWO_4$  or  $CaWO_4$ .

The internal oxygen bending motion,  $\nu_5$  that falls between  $400\text{--}500\text{ cm}^{-1}$  is the second strongest set of peaks in the spectra. If the  $A_g$  and  $B_g$  components cannot be resolved then the  $\nu_5$  mode is expected to split into a triplet. As shown in Figure 5, the  $\nu_5$  mode is clearly split into a doublet in  $Sr_2ZnWO_6$  and  $Ca_2CaWO_6$ . The splitting is more difficult to resolve in the other three compounds. Why the splitting should be seen most easily in the compounds that have the largest and smallest tolerance factors of the group, respectively, is not clear.

Proceeding to lower wavenumbers, the libration lattice modes are the next peaks expected to appear. In a perovskite with  $P2_1/n$  symmetry, six libration lattice modes are predicted, three  $A_g$  and three  $B_g$  modes.  $Sr_2ZnWO_6$  does not appear to have any librational modes that are strong enough to be seen above the background. Lenz reported peaks in this area of the spectrum in his study of  $Sr_2ZnWO_6$ , but they were extremely weak, thus explaining the absence of visible libration modes in our spectra [26].  $Sr_2CdWO_6$ ,  $Ca_2MgWO_6$  and  $Ca_2CaWO_6$  all have a peak of moderate intensity near  $250\text{ cm}^{-1}$  that we assign as a libration mode  $L$ . Curiously this peak is too weak to be observed in  $Sr_2CaWO_6$ . Additionally most of the compounds have weak peaks between  $390$  and  $420\text{ cm}^{-1}$  that cannot be unambiguously assigned as being either an external libration mode or an internal bending mode.

**Table 4:** Raman shifts (in  $\text{cm}^{-1}$ ) for the observed modes in the tungsten double perovskites with  $P2_1/n$  symmetry.

Assignment	$Sr_2ZnWO_6$	$Sr_2CdWO_6$	$Sr_2CaWO_6$	$Ca_2MgWO_6$	$Ca_2CaWO_6$
T	137	129	110	149	132
T	152	151	126	165	144
T	170	172	134	176	193
T	–	190	150	192	207
T	–	–	173	212	218
T	–	–	195	–	–
L	–	246	–	249	247
L	–	–	–	304	256
L	–	–	–	330	301
$\nu_5$ or L	–	390	395	406	–
$\nu_5$ or L	–	411	415	424	416
$\nu_5$	436	440	441	472	453
$\nu_5$	445	465	465	–	465
$\nu_2$	573	554	583	584	594
$\nu_1$	855	824	818	836	811
$AWO_4$	921	921, 800, 371, 336	922	908, 331	–

The translation lattice modes are expected at the lowest frequencies. In a perovskite with  $P2_1/n$  symmetry, six translation lattice modes are predicted, via a triplet splitting of the  $A_g$  and  $B_g$  modes. Where the libration modes end and the translation modes begin is not completely clear. Polarized Raman and infrared spectra are needed to accurately differentiate libration and translation lattice modes. In a study of  $A_2CoM'O_6$  ( $A = Sr, Ca; M' = W, Te$ ) Ayala *et al.* assigned the libration lattice modes to frequencies in the range  $190\text{--}310\text{ cm}^{-1}$ , and translation lattice modes to frequencies less than  $190\text{ cm}^{-1}$  for  $P2_1/n$  double perovskites [24], but as discussed below there is some evidence that the translation lattice modes may extend as high as  $220\text{ cm}^{-1}$  in these compounds.

Lenz previously reported the Raman spectra for  $Sr_2ZnWO_6$  ( $t = 0.976$ ), which showed weak bands at  $78, 105, \text{ and } 116\text{ cm}^{-1}$ , the first of these is outside of the range of our spectrometer, while the latter two are not observed in this study. Lenz also observed modes at  $140$  and  $153\text{ cm}^{-1}$ , corresponding to the translational lattice modes that are observed here [23]. There is a broad tailing that occurs on the high frequency side of the doublet, centered approximately at  $170\text{ cm}^{-1}$  and it is possible that this broad feature may correspond to a third translational mode. Looking back at Table 3, the Zn–O–W angles range from  $164^\circ$  to  $168^\circ$ , which are the least bent of all the  $P2_1/n$  perovskites considered here. It could be argued that the relatively small magnitude of octahedral tilting leads to less splitting of the translational modes in this compound than the other  $P2_1/n$  perovskites. The close proximity to the  $P2_1/n \rightarrow I4/m$  phase transition at  $343\text{ K}$  (see Table 1) may also play a role in making the splitting of the translational modes too subtle to resolve.

$Sr_2CdWO_6$  ( $t = 0.930$ ) shows a definitive triplet splitting with peaks at  $129, 151, 172\text{ cm}^{-1}$ , and a fourth very weak peak at  $190\text{ cm}^{-1}$ . The lower tolerance factor leads to more distorted Cd–O–W bonds, with angles that range from  $152^\circ$  to  $159^\circ$ .  $Sr_2CaWO_6$ , which has the same A-site cation and a similar tolerance factor ( $t = 0.916$ ), has four translational modes that

fall at nearly the same wavenumbers, as well as additional weak peaks at 110 and 134  $\text{cm}^{-1}$ . These values are in good agreement with those reported by Gateshki and Igartua [27].

Coming to  $\text{Ca}_2\text{MgWO}_6$  the tolerance factor lies in the same range ( $t = 0.926$ ) but the A-site cation is now  $\text{Ca}^{2+}$  instead of  $\text{Sr}^{2+}$ . Since the translational modes involve motions of the A-site cation the lighter mass of the  $\text{Ca}^{2+}$  ion (40.1 vs. 87.6 amu) should result in a shift of these modes to higher frequencies. Based on that expectation five peaks between 149 and 212  $\text{cm}^{-1}$  are tentatively assigned as translational modes. If this assignment is correct the modes shift to higher frequencies by 20 to 40  $\text{cm}^{-1}$  when  $\text{Sr}^{2+}$  is replaced by  $\text{Ca}^{2+}$ .

Finally,  $\text{Ca}_2\text{CaWO}_6$ , which has the smallest tolerance factor ( $t = 0.867$ ) and more highly bent M–O–W bonds ( $141^\circ$  to  $147^\circ$ ), also appears to have five translational modes that fall in a similar region of the spectrum, but the increased distortion of the structure leads to clear differences in the intensities and frequencies of these modes with respect to  $\text{Ca}_2\text{MgWO}_6$ .

Preliminary results obtained from force constant calculations show that considerable coupling occurs between the lower-lying wavenumber bands of these solids. Unfortunately because they are both weak and numerous unambiguous assignments cannot be made without the availability of single crystal Raman and infrared data.

## Discussion

The frequency of the symmetric stretch,  $\nu_1$ , is plotted as a function of tolerance factor in Figure 6 for the seven compounds studied here, as well as an additional seven  $\text{A}_2\text{MWO}_6$  double perovskites— $\text{Ba}_2\text{NiWO}_6$  [23],  $\text{Ba}_2\text{ZnWO}_6$  [23],  $\text{Ba}_2\text{MnWO}_6$  [28],  $\text{Sr}_2\text{MgWO}_6$  [29],  $\text{Sr}_2\text{CoWO}_6$  [24],  $\text{Sr}_2\text{MnWO}_6$  [28], and  $\text{Ca}_2\text{CoWO}_6$  [24]. The tolerance factors and frequencies of the  $\nu_1$  and  $\nu_5$  bands for these additional compounds are given in the supporting information (Table S2). The frequency of the  $\nu_1$  mode does not appear to be very sensitive to the identity of the A cation, nor to the mass of the M cation, as expected for an internal mode of the octahedron that does not involve motion of the cations. However, it does show a dependence on the tolerance factor.

The cubic double perovskites with tolerance factors larger than one have relatively low frequency symmetric stretches (810 – 822  $\text{cm}^{-1}$ ). Once the tolerance factor drops below one and octahedral tilting distortions set in, the frequency of the  $\nu_1$  mode spikes. This result can be understood in the following manner. In those  $\text{A}_2\text{MWO}_6$  double perovskites where the tolerance factor is larger than one, the octahedra are stretched by the oversized A-site cation. This effect weakens the M–O and/or the W–O bonds, thereby lowering the energy of the oxygen ion vibration along the M–O–W axis.

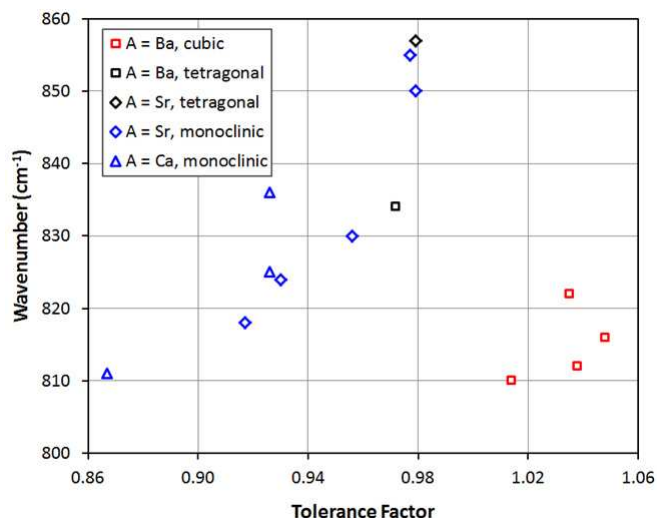


**Figure 6:** Frequencies of the oxygen symmetric stretch  $\nu_1$  as a function of tolerance factor for  $\text{A}_2\text{MWO}_6$  double perovskites.

To support this hypothesis consider Table 5, which contains the bond valence sums for each of the five  $\text{Ba}_2\text{MWO}_6$  compounds included in Figure 6. Only in  $\text{Ba}_2\text{CaWO}_6$  ( $t = 0.972$ ) does the bond valence sum of tungsten exceed its ideal value of 6, and the  $\text{Ca}^{2+}$  ion is also overbonded in this compound. Despite the tetragonal symmetry the bonds are still quite close to linear in this compound (see Table 3). Given the fact that both the M–O and W–O bonds are effectively compressed from their ideal values, it should not come as a surprise that the position of the symmetric stretch is 12–22  $\text{cm}^{-1}$  higher than it is in the other  $\text{Ba}_2\text{MWO}_6$  compositions.

**Table 5:** Space group symmetry, tolerance factor, symmetric stretching frequency, and bond valence sums for  $\text{Ba}_2\text{MWO}_6$  double perovskites.

Compound	Tolerance Factor	$\nu_1$ ( $\text{cm}^{-1}$ )	Bond valence sums			
			Ba	$\text{M}^{2+}$	W	O
$\text{Ba}_2\text{NiWO}_6$	1.048	816	2.58	1.81	5.70	2.11
$\text{Ba}_2\text{MgWO}_6$	1.038	812	2.49	1.88	5.87	2.12
$\text{Ba}_2\text{ZnWO}_6$	1.035	822	2.45	1.87	5.88	2.11
$\text{Ba}_2\text{MnWO}_6$	1.014	810	2.27	2.11	5.90	2.09
$\text{Ba}_2\text{CaWO}_6$	0.972	834	1.87	2.57	6.02	2.06

Once octahedral tilting has set in a further decrease in the tolerance factor leads to a decrease in the energy of the  $\nu_1$  symmetric stretching mode. This trend can also be rationalized by taking into account how the structure changes as the tolerance factor continues to decrease. Because the W–O bonds are easily the strongest bonds in these compounds the internal  $\nu_1$  mode can be thought of as a vibration of the  $[\text{WO}_6]^{6-}$  octahedra. When the W–O–M bonds are linear an expansion in the W–O bond leads to an equivalent compression of the M–O bonds, and vice versa. However, as the tolerance factor decreases the M–O–W bonds become increasingly bent. Once the W–O–M bonds are bent an expansion of the bonds in each



$[\text{WO}_6]^{6-}$  octahedron does not lead to a pure compression of the M–O bonds, but rather a mixture of compression and bending. As a general rule bending modes are lower energy than stretching modes, hence there is less resistance to changes in the W–O bond lengths when the M–O–W bonds are bent.

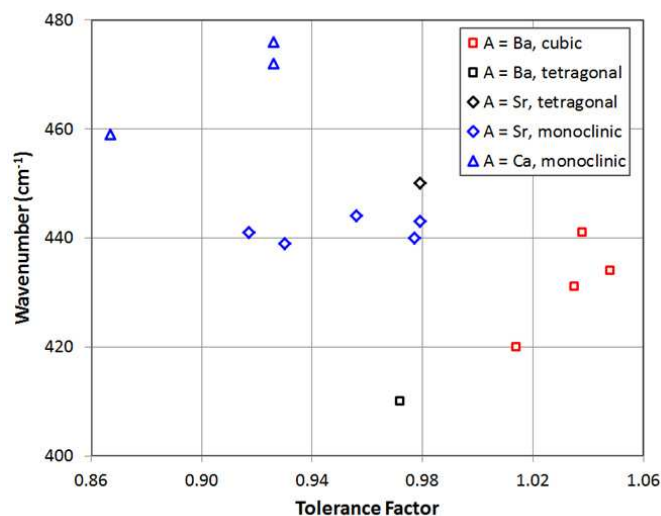


**Figure 7:** Frequencies of the oxygen bending mode  $\nu_5$  as a function of tolerance factor for  $\text{A}_2\text{MWO}_6$  double perovskites.

Plotting the frequencies of the  $\nu_5$  bending mode tells a different story, as shown in Figure 7. The frequencies for double perovskites with A = Sr cluster into a narrow range of values that fall between 439–450  $\text{cm}^{-1}$ . The frequency of the bending mode shifts to higher values when A = Ca, and lower values when A = Ba. The relative order  $\nu_5(\text{A} = \text{Ba}) < \nu_5(\text{A} = \text{Sr}) < \nu_5(\text{A} = \text{Ca})$  mirrors the relative masses of the three A-site cations, and is a clear sign that a motion of the A-site cation must also be involved in the oxygen bending mode. Returning to the group theory discussed earlier we see that this coupling of internal and external modes is allowed because the oxygen bending mode and the A-site cation translation mode have one or more common irreducible representations for all three space group symmetries. Thus it is not completely accurate to describe this mode as a pure internal vibration of the octahedron.

The frequency of the  $\nu_5$  mode for the Ba-containing double perovskites shows some dependence on tolerance factor. Once again the bond valence sums shown in Table 5 are illustrative. Because the oxygen bending mode leads to changes in the A–O bond lengths, its frequency should increase as the  $\text{Ba}^{2+}$  ion becomes increasingly overbonded. Table 5 and Figure 7 show that as the tolerance factor increases so does the valence of the  $\text{Ba}^{2+}$  ion and hence the frequency of the  $\nu_5$  mode.

## Conclusions

As the symmetry is lowered from cubic  $Fm\bar{3}m$  to monoclinic  $P2_1/n$  additional peaks appear in the Raman spectrum, as predicted by group theory. However, it is not possible to observe/resolve all 24 peaks that are predicted in spectra taken on polycrystalline samples. The lone tetragonal  $I4/m$  compound that was studied,  $\text{Ba}_2\text{CaWO}_6$ , did not exhibit any peaks in its Raman spectrum that would signal a lowering of the symmetry from cubic to tetragonal. The frequency of the oxygen symmetric stretch  $\nu_1$  is relatively low for cubic perovskites with tolerance factors larger than one, but increases sharply as the tolerance factor drops below one and octahedral tilting sets in ( $t \approx 0.98$ ). Further decreases in tolerance factor lead to a more gradual decrease in the frequency of the  $\nu_1$  mode. The frequency of the oxygen bending mode  $\nu_5$  increases as the mass of the A cation decreases. This observation is clear evidence that the  $\nu_5$  vibrational mode of the  $[\text{WO}_6]^{6-}$  octahedron, strongly couples to one or more external lattice modes.

## Acknowledgements

Financial support from the National Science Foundation (Award number DMR-0907356) is acknowledged.

## Notes and references

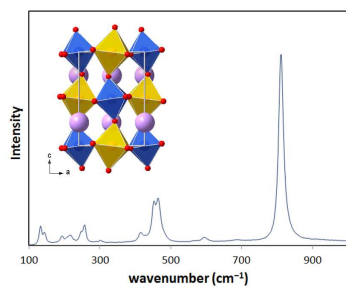
<sup>a</sup> Department of Chemistry and Biochemistry, The Ohio State University, 100 W. 18<sup>th</sup> Avenue, Columbus, OH 43210-1106 USA.

Electronic Supplementary Information (ESI) available: lattice parameters determined from Rietveld refinements of X-ray powder diffraction data, values of  $\nu_1$  and  $\nu_5$  modes for  $\text{A}_2\text{MWO}_6$  perovskites studied in the literature, and Raman spectra of  $\text{AWO}_4$  scheelite phases.

- 1 M. T. Anderson, K. B. Greenwood, G. A. Taylor, K. R. Poeppelmeier, *Prog. Solid State Chem.* 1993, **22**, 197.
- 2 M. W. Lufaso, P. W. Barnes, P. M. Woodward, *Acta Cryst. B* 2006, **62**, 397.
- 3 S. Vasala, M. Karppinen, *Prog. Solid State Chem.* 2014, (in press) <http://dx.doi.org/10.1016/j.progsolidstchem.2014.08.001>
- 4 A. A. Bokov, Z.-G. Ye, *J. Mater. Sci.* 2006, **41**, 31.
- 5 A. Dias, G. Subodh, M. T. Sebastian, R. L. Moreira, *J. Raman Spect.* 2010, **41**, 702.
- 6 J. B. Goodenough, Y. H. Huang, *J. Power Sources*, 2007, **173**, 1.
- 7 K. L. Kobayashi, T. Kimura, H. Sawada, K. Terakura, Y. Tokura, *Nature* 1998, **395**, 677.
- 8 P. M. Woodward, *Acta Cryst. B* 1997, **53**, 44.
- 9 M. W. Lufaso, P. M. Woodward, *Acta Cryst. B* 2001, **57**, 725.
- 10 G. King, P. M. Woodward, *J. Mater. Chem.* 2010, **20**, 5785.
- 11 P. W. Barnes, M. W. Lufaso, P. M. Woodward, *Acta Cryst. B* 2006, **62**, 384.
- 12 C. J. Howard, B. J. Kennedy, P. M. Woodward, *Acta Cryst. B* 2003, **59**, 463.

- 13 R. W. Cheary, A. Coelho, *J. Appl. Cryst.* 1992, **25**, 109.
- 14 A. M. Glazer, *Acta Cryst. B* 1972, **28**, 3384.
- 15 K. Yamamura, M. Wakeshima, Y. Hinatsu, *J. Solid State Chem.* 2006, **179**, 605.
- 16 W. T. Fu, Y. S. Au, S. Akerboom, D. J. W. IJdo, *J. Solid State Chem.* 2008, **181**, 2523.
- 17 B. E. Day, N. D. Bley, H. R. Jones, R. M. McCullough, H. W. Eng, S. H. Porter, P. M. Woodward, P. W. Barnes, *J. Solid State Chem.* 2012, **185**, 107.
- 18 M. Gateshki, J. M. Igartua, E. Hernandez-Bocanegra, *J. Phys. Cond. Matter* 2003, **15**, 6199.
- 19 A. Faik, J. M. Igartua, J. L. Pizarro, *J. Molec. Struct.* 2009, **920**, 196.
- 20 J. H. Yang, W. K. Choo, C. H. Lee, *Acta Cryst. C* 2003, **59**, 86.
- 21 G. Madariaga, A. Faik, T. Brezczewski, J. M. Igartua, *Acta Cryst. B* 2010, **66**, 109.
- 22 J. A. Alonso, M. J. Martinez-Lopez, M. T. Casais, M. T. Fernandez-Diaz, *Inorg. Chem.* 2000, **39**, 917
- 23 M. Liegeois-Duyckaerts and P. Tarte, *Spectrochimica Acta* 1974, **30A**, 1771
- 24 A. P. Ayala; I. Guedes; E. N. Silva, *J. Appl. Phys.* 2007, **101** 123511-1.
- 25 J. R. Ferraro; K. Nakamoto; C. W. Brown, *Introductory Raman Spectroscopy*. Academic Press, New York, 2003.
- 26 V. A. Lentz, *Z. Anorg. Allg. Chem.* 1973, **402**, 153.
- 27 M. Gateshki, J. M. Igartua, *J. Phys. Cond. Matter*, 2004, **16**, 6639.
- 28 Y. Fujioka, J. Frantti, M. Kakihana, *J. Phys. Chem. B* 2006, **110**, 777.
- 29 B. Manoun, A. Ezzahi, S. Benmokhtar, L. Bihc, Y. Tamraoui, R. Haloui, F. Mirinioui, S. Addakiri, J.M. Igartua, P. Lazor, *J. Molec. Struct.* 2013, **1045**, 1.

## Graphical Abstract



The Raman spectra of  $A_2MWO_6$  double perovskites with various symmetries have been studied.